



# Elementary Processes and Mechanisms of Interactions of Antimicrobial Peptides with Membranes—Single Giant Unilamellar Vesicle Studies—

Moynul Hasan and Masahito Yamazaki

## Abstract

To elucidate the mechanisms of action of antimicrobial peptides (AMPs) and to develop de novo designed peptides with activities similar to those of AMPs, it is essential to elucidate the detailed processes of AMP interactions with plasma membranes of bacterial and fungal cells and model membranes (lipid bilayers). In this mini-review, we summarize the present state of knowledge of the interactions of AMPs with lipid vesicles obtained using the single giant unilamellar vesicle (GUV) method. Currently, three modes of action of AMPs on GUVs have been defined. The elementary processes of interactions of AMPs with lipid vesicles revealed by the single GUV method, and the advantages of this technique, are described and discussed. For example, the single GUV method can be used to determine

rate constants of AMP-induced pore formation or local rupture and membrane permeation of internal contents through the pore or the local rupture, the transbilayer movement of lipids, and the relationship between the location of AMPs and pore formation. Effects of membrane tension and of asymmetric lipid packing in the bilayer on AMP-induced pore formation also are described. On the basis of these data, we discuss the present state of understanding of the interaction of AMPs with lipid bilayers and future prospects for AMP studies.

## Keywords

Antimicrobial peptides · Giant unilamellar vesicle · Pore formation · Local rupture · Translocation across membranes · Lipid bilayers · Elementary process · Rate constant · Membrane tension

M. Hasan  
Integrated Bioscience Section, Graduate School of Science and Technology, Shizuoka University, Shizuoka, Japan

M. Yamazaki (✉)  
Integrated Bioscience Section, Graduate School of Science and Technology, Shizuoka University, Shizuoka, Japan

Nanomaterials Research Division, Research Institute of Electronics, Shizuoka University, Shizuoka, Japan

Department of Physics, Graduate School of Science, Shizuoka University, Shizuoka, Japan  
e-mail: [yamazaki.masahito@shizuoka.ac.jp](mailto:yamazaki.masahito@shizuoka.ac.jp)

## 3.1 Introduction

Antimicrobial peptides (AMPs) and antimicrobial proteins with bactericidal and fungicidal activities are produced by various organisms (e.g., animals including humans, plants, and insects) to defend themselves against microbes. Most AMPs target bacterial and fungal plasma membranes and induce damage in the membranes,

including pore formation that increases membrane permeability (Zasloff 2002; Melo et al. 2009; Hwang and Vogel 1998; Propheter et al. 2017). Some AMP-induced damage to the plasma membrane is considered to reflect the interaction of these AMPs with the lipid membrane regions of bacterial and fungal plasma membranes, as indicated by the observation that synthetic AMP analogues composed of all-D amino acids have the same antibacterial activity as wild-type AMPs composed of all-L amino acids (Wade et al. 1990; Wakabayashi et al. 1999).

It has been established that the physicochemical properties of lipid bilayer vesicles are similar to those of native plasma membranes, and lipid bilayers are therefore excellent models of plasma membranes (Lipowsky and Sackmann 1995; Baumgart et al. 2003; McLaughlin and Murray 2005; Bigay and Antonny 2012). To investigate the interaction of AMPs with the lipid membrane regions of microbial plasma membranes, various kinds of vesicles composed of lipid bilayers have been extensively used. To date, most research on the interactions of AMPs with lipid bilayers has been performed using suspensions of large unilamellar vesicles (LUVs) with a diameter of 50 nm–1  $\mu$ m (100–300 nm for most uses) (i.e., the LUV suspension method). Given their small size, we cannot observe the structure and the physical quantities of each LUV in buffer; hence, using the LUV suspension method, we can obtain only ensemble averages of physical quantities of many LUVs in a suspension, as measured by various biophysical and physicochemical techniques. Therefore, the LUV suspension technique does not permit observation of each elementary process in the interaction of peptides such as AMPs with lipid bilayers (Yamazaki 2008; Islam et al. 2018). In contrast, the shape and physical properties of each giant unilamellar vesicle (GUV) with a diameter larger than 1  $\mu$ m (10–40  $\mu$ m for most uses) in buffer can be observed in real time using various optical microscopy techniques. Using this advantage, GUVs have been employed to investigate shape changes, the elastic modulus of lipid bilayers, phase separation, and tension-induced pore formation (Sandre et al. 1999; Rawicz et al. 2000; Baumgart et al. 2003; Tanaka et al. 2004).

We recently developed the single GUV method to investigate interactions of compounds such as peptides/proteins with lipid bilayers (Tamba and Yamazaki 2005, 2009; Yamazaki 2008; Tamba et al. 2010; Islam et al. 2014a, b, 2018). In this method, performed under various optical microscopes, a compound solution is delivered continuously to the vicinity of a single GUV through a micropipette to induce the interaction of the compound with the single GUV. During the interaction, changes in the structure and physical properties of the single GUV are measured as a function of time and spatial coordinates using fluorescence microscopy coupled with an electron-multiplying charge-coupled device (EM-CCD) camera and confocal laser scanning microscopy (CLSM). We perform the same experiment using many “single GUVs” under the same conditions and then analyze the results statistically (Yamazaki 2008; Islam et al. 2018). The single GUV method enables us to distinguish the elementary processes of individual events occurring in a single GUV during the interaction of an AMP with the GUV, and statistical analysis permits us to derive the rate constants of each elementary process.

In this mini-review, we focus on research on the interactions of AMPs with lipid vesicles using the single GUV method. We review what kinds of new information on the interaction of AMPs with lipid bilayers have been obtained using the single GUV method, compared with the information obtained using the LUV suspension method. Here, as the examples of AMPs, we use magainin 2, lactoferricin B (LfcinB), LfcinB (4–9) (which has the amino acid sequence RRWQWR, making this AMP one of the shortest versions of LfcinB), and transportan 10 (TP10). Among these examples, TP10 is not a native AMP because this molecule is a synthetic, cell-penetrating peptide (CPP). However, TP10 has been shown to exhibit strong antimicrobial activity while being able to enter eukaryotic cells without affecting viability (Nekhotiaeva et al. 2004). Hence, we can reasonably infer that TP10 has an activity similar to AMPs, given that TP10 induces preferential damage in microbes.

### 3.2 Mode of Action of AMPs

To date, three distinct modes of action (MoAs) of AMPs on lipid bilayers have been observed using the single GUV method: (A) small pore formation, (B) local rupture and complete rupture (or burst), and (C) no damage to the bilayers. In the type A MoA, AMPs induce small pores in lipid bilayers; these pores cannot be observed using optical microscopy but can be detected by the membrane permeation (i.e., leakage) of water-soluble fluorescent probes from the lumen of single GUVs to the outside. After the leakage, the same spherical GUVs without any detectable breaks remain, and their sizes do not change significantly. First, we consider the results for magainin 2. The magainin 2-induced leakage of internal contents has been extensively investigated using the LUV suspension method (Matsuzaki et al. 1995, 1998; Gregory et al. 2009). Those studies indicated that magainin 2 induces leakage of water-soluble fluorescent probes from the lumen of LUVs, suggesting that magainin 2 induces pores in lipid membranes. However, there are several factors (such as pore formation, membrane fusion, large change in local curvature, rupture, and fragmentation of the liposomes) that induce leakage of the internal contents from vesicle lumens, and it is difficult to clearly identify the cause of leakage using the LUV suspension method (Yamazaki 2008). Figure 3.1a shows a result for the magainin 2-induced leakage of a water-soluble fluorescent probe, calcein, from single GUVs composed of dioleoylphosphatidylglycerol (DOPG; hereafter PG) and dioleoylphosphatidylcholine (DOPC; hereafter PC) (Tamba and Yamazaki 2005, 2009). The fluorescence intensity (FI) of the GUV lumen in the fluorescence microscopic images (Fig. 3.1a (II)) was proportional to calcein concentration in the lumen. The time course of the change in FI indicated that the calcein began to leak from the lumen suddenly after an extended time of interaction, and this leakage continued gradually (Fig. 3.1b). During this leakage, local disruption, rupture of the GUVs, changes in local curvature of the membrane, membrane fusion, and vesicle fission did not occur, indicating that

magainin 2 formed pores in the membrane through which the membrane permeation of calcein occurred. Hence, the MoA of magainin 2 is type A. Similarly, lysenin, a pore-forming toxin (PFT) protein, induced gradual membrane permeation of calcein from GUVs of lipid bilayers composed of sphingomyelin (SM), PC, and cholesterol (chol) (Alam et al. 2012); the MoA of lysenin also is type A.

In the type B MoA, AMPs induce local rupture or complete rupture of single GUVs, through which fluorescent probes rapidly leak away. After the leakage, the size of GUVs decreases a little, and sometimes several partially thickened membranes appear at the rim of the GUVs (corresponding to the GUV membranes). First, we consider the results for LfcinB. Figure 3.2a shows the result of LfcinB-induced leakage of calcein from single PG/PC-GUVs (Moniruzzaman et al. 2015). The calcein began to leak from the lumen suddenly after an extended time of the interaction, and the leakage then was completed within several seconds (Fig. 3.2a, c), after which the spherical GUV structure remained, albeit with a decreased diameter. These observations indicate the occurrence of a local rupture or a large pore in the GUV membrane, and hence, LfcinB belongs to type B. In the case of the interaction of TP10 with single GUVs, a transient local rupture was sometimes observed, although the rate of leakage was slower than that observed with LfcinB (Islam et al. 2014a). On the other hand, epigallocatechin gallate (EGCg), a tea catechin (antimicrobial substance), induced rapid leakage of calcein from single PC-GUVs within a few seconds, and after this leakage, the spherical GUVs were converted to single smaller lumps composed of lipid and EGCg (Tamba et al. 2007). During the conversion, we observed a large pore in a GUV membrane using optical microscopy. In this case, no spherical GUVs remained after the leakage, and therefore, we can infer that EGCg induces rupture of GUVs.

In the type C MoA, AMPs do not induce any significant damage in lipid bilayers, and hence no leakage of fluorescent probes occurs; however, AMPs translocate across lipid bilayers to

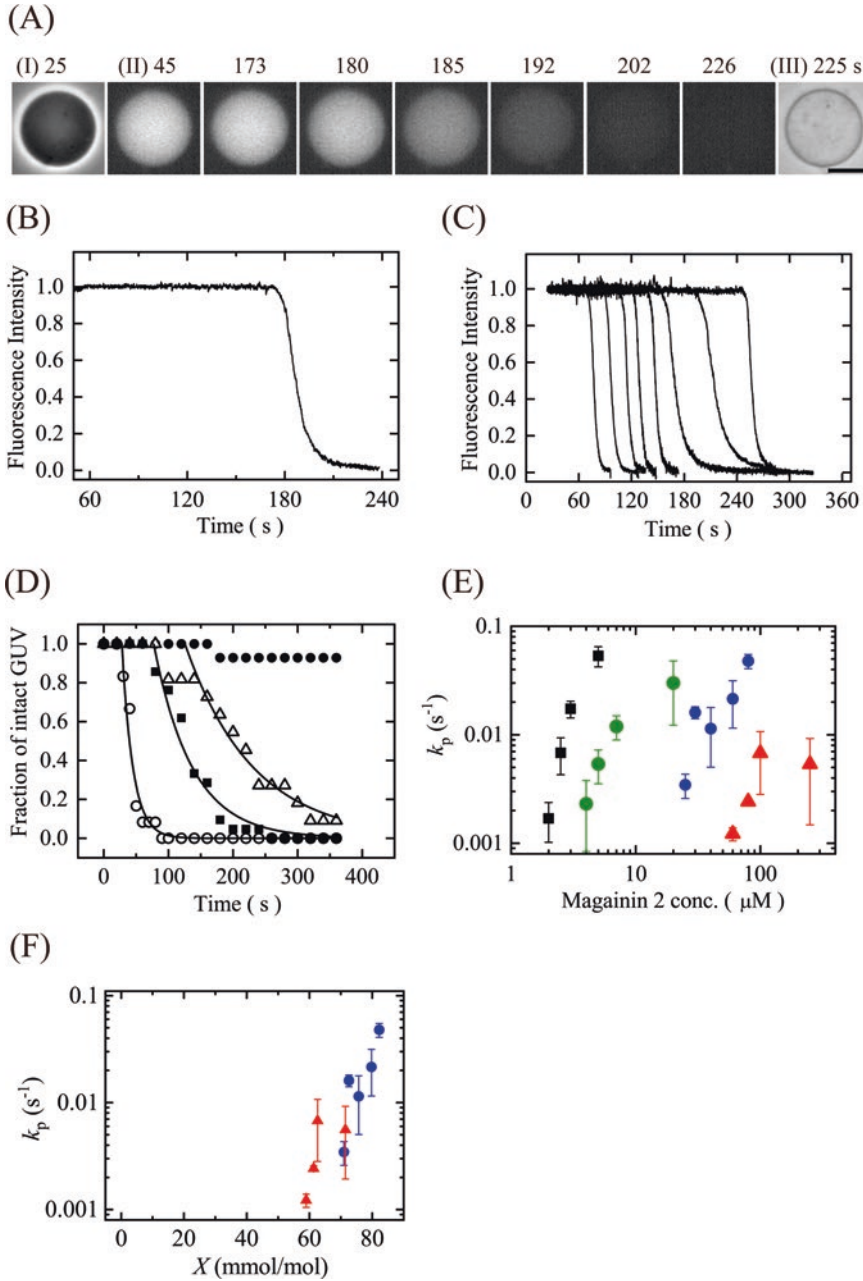


**Fig. 3.1** Magainin 2-induced membrane permeation of calcein from single GUVs. Buffer A (10 mM PIPES, pH 7.0, 150 mM NaCl, 1 mM EGTA) was used at 25 °C. (a) Fluorescence images (II) show the time course of the FI due to calcein in a PG/PC (6/4)-GUV lumen during the interaction with 3  $\mu\text{M}$  magainin 2. The numbers above each image show the time in seconds after the magainin 2 addition was started. Also shown are phase-contrast images of the GUV (I, III). The bar corresponds to 10  $\mu\text{m}$ . (b) Time course of the change in the normalized FI of the GUV shown in (a). (c) Other examples of the time course of the change in FI of single GUVs under the same condi-

tions as in (a). (d) Time course of  $P_{\text{intact}}$  of PG/PC (6/4)-GUV in the presence of various concentrations of magainin 2: (○) 5, (■) 3, (△) 2.5, and (●) 1  $\mu\text{M}$ . The solid lines represent the best fit curves of Eq. 3.1. (e) Dependence of the rate constant of pore formation,  $k_p$ , on magainin 2 concentration in buffer. C. (■), PG/PC (6/4)-; (green ●), PG/PC (5/5)-; (blue ●), PG/PC (4/6)-; and (red ▲), PG/PC (3/7)-GUVs. (f) Dependence of  $k_p$  on  $X$  (a–e and f are reprinted from Tamba and Yamazaki 2009; Karal et al. 2015, respectively, with permission from the American Chemical Society)

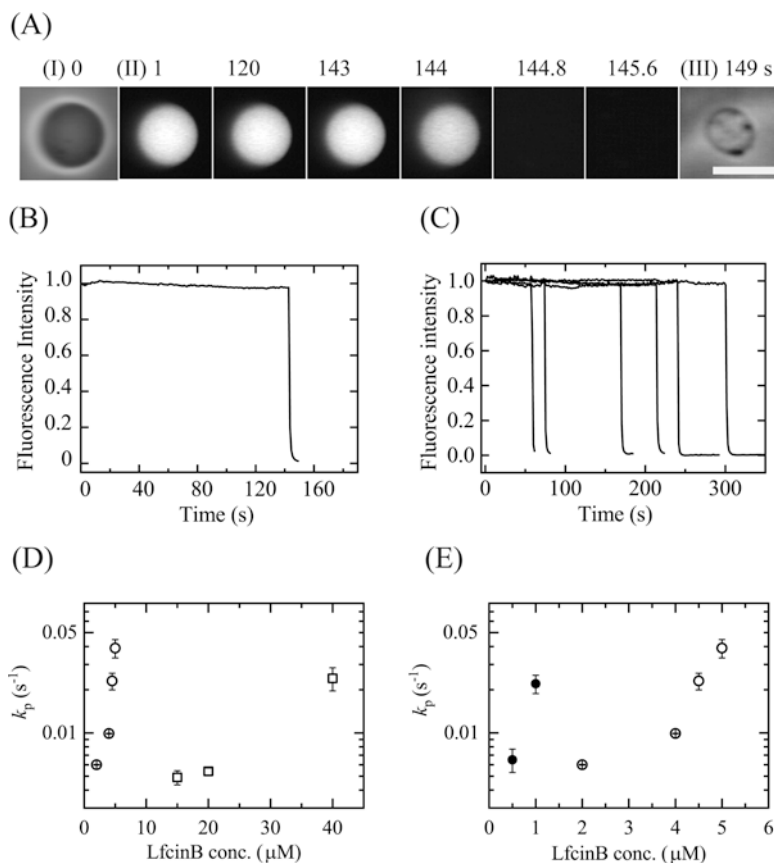


**Fig. 3.2** LfcinB-induced membrane permeation of calcein from single GUVs. Buffer A was used at 25 °C. (a) Fluorescence images (II) show the time course of the FI due to calcein in a PG/PC (1/1)-GUV lumen during the interaction with 2.0 μM LfcinB. The numbers above each image show the time in seconds after the LfcinB addition was started. Also shown are phase-contrast images of the GUV (I, III). The bar corresponds to 20 μm. (b) Time course of the change in the normalized FI of the GUV shown in (a). (c) Other examples of the time course of the

change in the FI of single GUVs. (d) The LfcinB concentration dependence of the rate constant of pore formation,  $k_p$ , in PG/PC (1/4)-GUV (□) and PG/PC (1/1)-GUV (○). (e) The LfcinB concentration dependence of the  $k_p$  in PG/PC (1/1)-GUV in buffer A without NaCl (10 mM PIPES, pH 7.0, 1.0 mM EGTA) (●) and in buffer A containing 150 mM NaCl (○) (a–e are reprinted from Moniruzzaman et al. 2015 with permission from the American Chemical Society)

enter the vesicle lumen. Here, we consider the results for LfcinB (4-9). The interaction of LfcinB (4-9) with single PG/PC-GUVs did not induce any leakage of calcein or AF647 (another water-soluble fluorescent probe). Nonetheless, Rh-LfcinB (4-9), which is LfcinB (4-9) labeled with a fluorescent probe (lissamine rhodamine B red), was translocated across a GUV membrane and entered the GUV lumen without leak-

age of AF647 (Fig. 3.3a) (Moniruzzaman et al. 2017). Moreover, Rh-LfcinB (4-9) entered the cytoplasm of *E. coli* cells without leakage of calcein. These data indicated that the antimicrobial activity of LfcinB (4-9) is not the result of damage to plasma membranes. Since AMPs with a type C MoA exhibit cell penetration activity, they are similar to cell-penetrating peptides (CPPs).



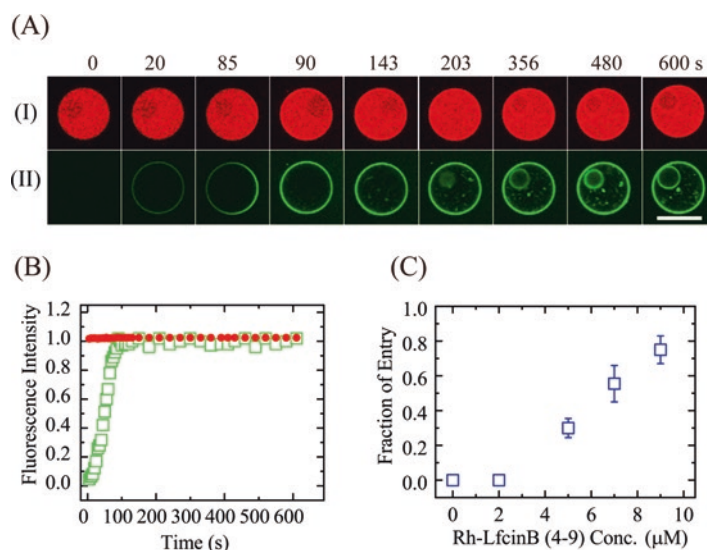


**Fig. 3.3** Entry of Rh-LfcinB (4-9) into single PG/PC (1/1)-GUVs containing small GUVs. Buffer A was used at 25 °C. (a) CLSM images of (I) AF647 and (II) Rh-LfcinB (4-9). The numbers above each image show the time in seconds after the addition of 5.0  $\mu\text{M}$  Rh-LfcinB (4-9) was started. The bar is 20  $\mu\text{m}$ . (b) Time course of the change in the normalized FI of the GUV during the interaction of

Rh-LfcinB (4-9) shown in (a). Red and green points correspond to the FI due to AF647 in the GUV lumen and due to Rh-LfcinB (4-9) in the rim of the GUV, respectively. (c) Dependence of  $P_{\text{entry}}$  (10 min) on the Rh-LfcinB (4-9) concentration (a–c are reprinted from Moniruzzaman et al. 2017 with permission from the American Chemical Society)

### 3.3 Advantages of the Single GUV Method

#### 3.3.1 Separation of Elementary Processes and Determination of the Rate Constant of Each Elementary Process

AMPs of types A and B induce membrane permeation of the internal contents via a mechanism that consists of at least two elementary processes. The first process is the AMP-induced damage in the membrane such as pore formation, local rupture, and burst; the second process is membrane permeation through the damage in the membrane. One of the largest disadvantages of the LUV suspension method is the inability to distinguish these two steps (Yamazaki 2008). On the other hand, the single GUV method enables us to separate these elementary processes of AMP-induced pore formation in the lipid bilayers and (local) rupture of GUVs.

First, we show the results for magainin 2. Figure 3.1a (II) shows fluorescence microscopic

images of a PG/PC (6/4)-GUV containing calcein in its lumen during the interaction with magainin 2. The time course of the FI of the GUV lumen due to calcein (Fig. 3.1b) provides two pieces of information: one is the time when pore formation starts in the membrane (based on the time at which the FI starts to decrease), and the other is the characteristics of membrane permeation of the fluorescent probe such as its rate constant (based on the time course of the decrease in FI after pore formation). If we perform the same experiments using multiple individual “single GUVs,” we can obtain more information. In the case of magainin 2, the membrane permeation of calcein from the single GUVs began stochastically (Fig. 3.1c), indicating that pore formation started stochastically in the lipid bilayers. Membrane permeation in each GUV was complete within a short time ( $\sim 30$  s under these conditions) after the start of membrane permeation (Fig. 3.1c). These results indicated that pore formation in the membrane is the rate-determining step in the total reaction of the magainin 2-induced leakage, because the other elementary

process (i.e., membrane permeation through the pore) is completed rapidly. This may correspond to the concept of the “all-or-none” mode of leakage in the LUV suspension method (Gregory et al. 2009). To analyze this type of stochastic phenomenon, the concept of a probability can be used; in this case, the probability is assessed as  $P_{\text{intact}}(t)$ , the fraction (among all examined GUVs) of intact GUVs where no membrane permeation of fluorescent probes occurs (Tamba and Yamazaki 2005, 2009).  $P_{\text{intact}}(t)$  decreased monotonically over time. If we apply an irreversible two-state transition model from the intact state to the pore state (i.e., the state of the GUV with pores), we can obtain the theoretical equation of the time course of  $P_{\text{intact}}(t)$  as follows:

$$P_{\text{intact}}(t) = \exp\{-k_p(t - t_{\text{eq}})\} \quad (3.1)$$

where  $k_p$  is the rate constant of the two-state transition, which can be considered as the rate constant of magainin 2-induced pore formation at the initial state, and  $t_{\text{eq}}$  is a fitting parameter and implies the time required to achieve the binding equilibrium of magainin 2 from aqueous solution to the GUV membrane. All the curves of the time courses of  $P_{\text{intact}}(t)$  were well fit to Eq. 3.1, providing the values of  $k_p$  (Fig. 3.1d). The rate constant  $k_p$  increased with an increase in magainin 2 concentration (Fig. 3.1e). Similarly, for AMPs with a type B MoA, we can obtain the rate constant of the two-state transition from the intact state to the rupture state (i.e., the rate constant of local rupture or complete rupture) from analysis of the time course of  $P_{\text{intact}}(t)$  using Eq. 3.1 (Moniruzzaman et al. 2015; Tamba et al. 2007). These rate constants also increased with increasing LfcinB and EGCg concentrations.

On the other hand, if we analyze the time course of the decrease in FI of the GUV lumen due to fluorescent probe after pore formation, we can obtain information on the AMP-induced membrane permeation such as the rate constant  $k_{\text{mp}}$  (Tamba and Yamazaki 2005; Tamba et al. 2010). The value of  $k_{\text{mp}}$  is determined as follows:

$$I_N(t) = I(t)/I(0) = \exp(-k_{\text{mp}}(t)t) \quad (3.2)$$

where  $I_N(t)$  is the normalized FI of the GUV lumen,  $I(t)$  is the FI of the GUV lumen at time  $t$  after initiation of membrane permeation, and  $I(0)$  is  $I(t)$  at  $t = 0$ . If we plot the log of  $I_N(t)$  as a function of time, the  $k_{\text{mp}}(t)$  can be obtained quantitatively from the slope of the curve. The value of  $k_{\text{mp}}$  depends on the radius of the GUVs ( $r$ ), but the membrane permeability coefficient,  $P(t)$ , which is derived from  $k_{\text{mp}}(t)$  (i.e.,  $P(t) = r k_{\text{mp}}(t)/3$ ), does not depend on the value of  $r$  (Alam et al. 2012).

### 3.3.2 Rate Constant of Pore Formation and Local Rupture

The rate constants of pore formation or local rupture greatly depend not only on AMP concentration in buffer but also on lipid composition and buffer conditions. As the concentration of the negatively charged lipid (such as PG) in the bilayers (i.e., the surface charge density of the membrane) increases, the  $k_p$  greatly increases (Figs. 3.1e and 3.2d). Moreover, as the concentration of the salt (e.g., NaCl) decreases, the  $k_p$  also greatly increases (Fig. 3.2e) (Tamba and Yamazaki 2009; Moniruzzaman et al. 2015). It is well recognized that electrostatic interactions due to the surface charges of lipid membranes in buffer increase with an increase in surface charge density or with a decrease in salt concentration (Israelachvili 1992). Therefore, these results clearly indicate that for magainin 2 and LfcinB, the values of  $k_p$  increase with an increase in electrostatic interactions.

Using the binding constant of magainin 2 to lipid bilayers, we can convert the magainin 2 concentration in the buffer,  $C$ , to the magainin 2 surface concentration in the membrane,  $X$  (mol/mol; the molar ratio of magainin 2 bound to the membrane interface to lipid in the outer monolayer of a GUV). Figure 3.1f shows the relationship between  $k_p$  and  $X$ . The dependences of  $k_p$  on  $X$  for GUVs with two different lipid compositions are largely superimposable, indicating that  $X$  determines the rate constant of magainin 2-induced pore formation (Tamba and Yamazaki 2009).

### 3.3.3 Rate Constant of Membrane Permeation

Generally, two factors (the size and the number of pores) determine the rate constant of membrane permeation of fluorescent probes through pores,  $k_{mp}$ . If we use various fluorescent probes of different sizes (Stokes-Einstein radius,  $R_{SE}$ ) for the AMP-induced membrane permeation experiment, we can determine the size of the AMP-induced pore and obtain information on the temporal change in pore size and the number of pores by analyzing the time course of  $k_{mp}$  (Tamba et al. 2010). In the case of magainin 2-induced pore formation in PG/PC (4/6)-GUVs, rapid membrane permeation of larger fluorescent probes [such as Texas-Red dextran 3000 (TRD-3k) ( $R_{SE} = 1.4$  nm) and Texas-Red dextran 10,000 (TRD-10k) ( $R_{SE} = 2.7$  nm)] occurred at the initial time, but the rate of membrane permeation subsequently decreased. Figure 3.4a shows more quantitative data for TRD-3k and TRD-10k. Using the two linear regions of these curves, we can obtain the values of  $k_{mp}$  at the initial stage ( $k_{mp}^{initial}$ ) and the final steady stage ( $k_{mp}^{steady}$ ). The value of  $k_{mp}^{initial}$  is 20–40 times greater than that of  $k_{mp}^{steady}$  under these conditions. In contrast, larger fluorescent probes [such as TRD-40k ( $R_{SE} = 5.0$  nm) and FITC-BSA ( $R_{SE} = 3.6$  nm)] leaked only at the initial stage of magainin 2-induced pore formation. Based on these results, we can reasonably conclude that magainin 2 initially induces a large, transient pore in lipid bilayers; within several minutes, the radius of the pore then decreases to a stable smaller size at the final steady stage. The result of no membrane permeation of Alexa-Fluor trypsin inhibitor (AF-SBTI) at the final stage with 7  $\mu$ M magainin 2 indicates that the radius of the pore at the final stage is smaller than 2.8 nm ( $R_{SE}$  of AF-SBTI) but is larger than 1.4 nm ( $R_{SE}$  of TRD-3k). This value agrees with the 1.9 nm radius of magainin 2-induced pores in multilayer membranes at equilibrium, as determined by neutron in-plane scattering (Ludtke et al. 1996). These data provide the first information concerning the kinetic pathway of AMP-induced pore formation in lipid bilayers (i.e., evolution of pores). Subsequently, other examples of the change in the size of pep-

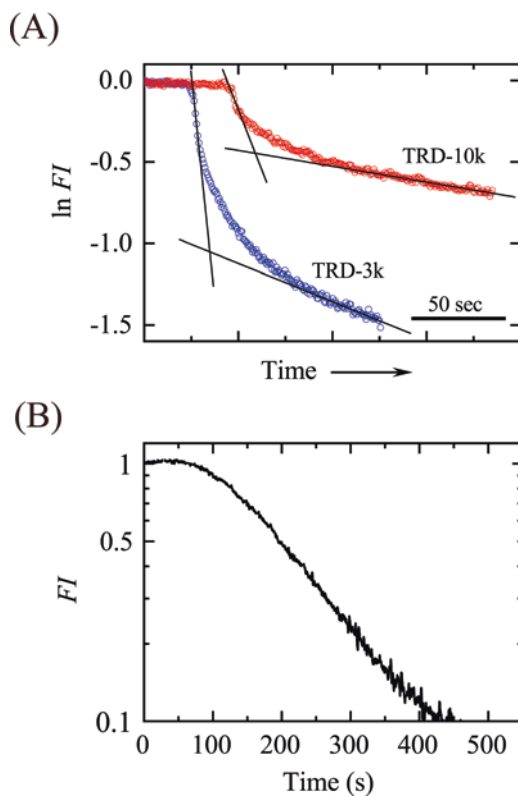


**Fig. 3.4** Time course of membrane permeation. (a) Magainin 2-induced membrane permeation of fluorescent probes from a PG/PC (1/1)-GUV. Time course of the logarithm of the normalized FI of the GUV containing TRD-3 k or TRD-10 k during the interaction with 4  $\mu$ M magainin 2 in buffer A at 25  $^{\circ}$ C. (b) Lysenin-induced membrane permeation of calcein from a SM/PC/chol (42/30/28)-GUV. Time course of the normalized FI of the GUV (log-10 scale) during the interaction with 40 ng/mL lysenin in PBS buffer at 37  $^{\circ}$ C (a, b are reprinted from Tamba et al. 2010; Alam et al. 2012, respectively, with permission from the American Chemical Society)

ptide-/protein-induced pores have been found using the GUV suspension method (Fuertes et al. 2010; Bleicken et al. 2013).

Contrast these results with those obtained with lysenin-induced membrane permeation of a small fluorescent probe, calcein ( $R_{SE} = 0.7$  nm), in single SM/PC/chol (42/30/28)-GUVs. After membrane permeation was initiated, the  $k_{mp}$  gradually increased with time before reaching a steady, maximum value, which persisted for an extended time (e.g., 280 s) (Fig. 3.4b) (Alam et al. 2012). This result indicated that after lysenin-induced pore formation began, the value



of  $P(t)$  increased with time before reaching a steady, maximum value of  $P^s$ , which was maintained for an extended time. Based on the experimental results that lysenin molecules form a specific oligomer in SM/PC/chol bilayers, we infer that these oligomers form pores with the same diameter. Therefore, the result of Fig. 3.4b indicated that the number of pores increased with time to reach the steady, maximum number.

### 3.3.4 Entry of AMPs Without Pore Formation

To detect the entry of AMPs into a GUV lumen with high sensitivity, we can use the single GUV method for CPPs. In this instance, we used CLSM to investigate the interaction of fluorescent probe-labeled AMPs with single GUVs containing smaller GUVs or LUVs and water-soluble fluorescent probes such as AF647 in their lumen (Islam et al. 2014a, 2018; Moghal et al. 2018). The binding of the fluorescent probe-labeled AMPs with bilayers of the small GUVs and LUVs increases their FI, and hence, we can detect the entry of the AMPs into the GUV lumen with higher sensitivity. The comparison between the FI of the GUV lumen due to water-soluble fluorescent probe and that due to fluorescent probe-labeled AMPs provides information on the relationship between the entry of AMPs and pore formation. Figure 3.3 shows a result for the interaction of Rh-LfcinB (4-9) with single PG/PC (1/1)-GUVs (Moniruzzaman et al. 2017). The FI of the GUV lumen due to AF647 remained constant (Fig. 3.3a (I) and red line in Fig. 3.3b) for 10 min, indicating no pore formation. On the other hand, the FI of small vesicles in the GUV lumen was observed after 143 s (Fig. 3.3a (II)), and the FI of the GUV membrane (i.e., the rim intensity) due to Rh-LfcinB (4-9) increased rapidly with time to reach a steady value at 100 s (Fig. 3.3b). These results indicated that Rh-LfcinB (4-9) first bound to the GUV membrane, then translocated across the bilayer, and finally entered into the GUV lumen without pore formation.

At present, the rate of entry of AMPs into the vesicle lumen is estimated as  $P_{\text{entry}}(t)$ , the fraction

of GUVs into which AMPs enter before a specific time  $t$ . Figure 3.3c indicates that  $P_{\text{entry}}$  (10 min) increased with an increase in Rh-LfcinB (4-9) concentration. It is also possible to estimate the rate constant of the binding of AMPs to the monolayer and the rate constant of unbinding by analyzing the rim intensity (Islam et al. 2014a, 2018).

### 3.3.5 AMP-Induced Transbilayer Movement of Lipids

The studies using the LUV suspension method suggested that the interactions of AMPs and venom peptides with lipid vesicles yielded an increase in  $k_{\text{FF}}$ , the rate constant of the transbilayer movement (i.e., flip-flop) of lipids (Matsuzaki et al. 1996; Müller et al. 2000). Matsuzaki et al. (1996) indicated a strong correlation between the magainin 2-induced leakage of internal contents and the flip-flop of lipids, suggesting the toroidal model of magainin 2-induced pore formation. Since the peptide-induced transbilayer movement of lipids is composed of several elementary steps, it was difficult to determine directly the main process for growth of  $k_{\text{FF}}$  in the framework of the LUV suspension method. On the other hand, the use of the single GUV method to measure the  $k_{\text{FF}}$  has an advantage (Hasan et al. 2018a, b). In this method, we use single GUVs with asymmetric lipid compositions in two monolayers, where a low concentration of fluorescent probe-labeled lipid [such as 18:1-NBD-lyso-PE (hereafter NBD-LPE)] exists only in their inner leaflet (e.g., PG/PC/NBD-LPE (40/59/1; inner leaflet)-PG/PC (40/59; outer leaflet)-GUVs). The analysis of the time course of the decrease in rim intensity due to NBD-LPE (measured using CLSM) provides the value of  $k_{\text{FF}}$ , because the rate of transfer of NBD-lipids from the outer leaflet to aqueous solution is large, and hence the rate-determining step of the decrease in rim intensity is the transbilayer movement of lipids from the inner leaflet to the outer one (Hasan et al. 2018b). In the interaction of magainin 2 with single GUVs with this asymmetric composition (Fig. 3.5), rim intensity decreased rapidly after the start of magainin

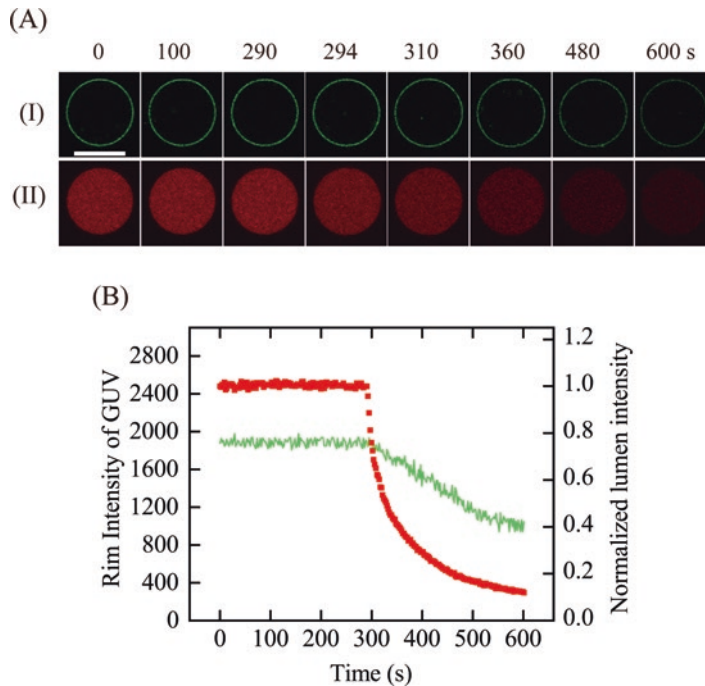


**Fig. 3.5** Relationship between the transbilayer movement of lipids and magainin 2-induced pore formation. (a) Relationship between the rim intensity of the GUVs due to NBD-LPE and the FI of the GUV lumen due to AF647 during the interaction of 31  $\mu\text{M}$  magainin 2 with PG/PC/NBD-LPE (40/59/1; inner)-PG/PC (40/59; outer)-GUVs. CLSM images of (I) NBD-LPE and (II) AF647. The num-

bers above each image show the time in seconds after magainin 2 addition was started. The bar corresponds to 20  $\mu\text{m}$ . (b) Time course of the change in FI of the GUV shown in (a). Red and green points correspond to the normalized FI of AF647 in the GUV lumen and the FI of NBD-LPE in the rim of the GUV, respectively

2-induced membrane permeation of AF647, indicating that the transbilayer movement of NBD-LPE occurred rapidly after pore formation, whereas before pore formation, the  $k_{\text{FF}}$  value was similar to that in the absence of magainin 2. This result clearly indicated that the occurrence of pores induced by magainin 2 increased the  $k_{\text{FF}}$  of NBD-LPE, whereas the binding of magainin 2 only to the membrane did not increase the  $k_{\text{FF}}$  value. The  $k_{\text{FF}}$  after pore formation was much larger than that in the normal lipid bilayer, indicating that the mechanism of the transbilayer movement of lipids after pore formation is different from that of normal transbilayer movement. If we assume that the structure of the magainin 2-induced pore at the initial stage is a toroidal pore, we can reasonably explain this great increase in  $k_{\text{FF}}$ . In a toroidal pore, the outer and inner monolayers bend and merge with each

other in a toroidal fashion to form a pore in which the inner wall is composed of peptides and lipid head groups (Matsuzaki et al. 1996; Ludtke et al. 1996; Yang et al. 2000; Qian et al. 2008). Therefore, lipid molecules can rapidly diffuse along this integrated lipid monolayer from the inner leaflet to the outer one through the wall of the pore, thereby inducing rapid transbilayer movement.

### 3.4 Relationship Between the Location of AMPs and Pore Formation

To elucidate the mechanism of AMP-induced pore formation, it is important to know the location of peptides in a lipid bilayer during pore formation. To elucidate the relationship between the

AMP-induced pore formation and the location of AMP in a GUV, interactions of fluorescent probe-labeled AMPs (e.g., carboxyfluorescein (CF)-labeled AMP) with single GUVs containing AF647 in their lumen have been investigated using CLSM. At present, we have defined two kinds of relationships: (A) asymmetric transmembrane distribution of AMPs before pore formation (e.g., as with magainin 2) and (B) symmetric transmembrane distribution of AMPs before pore formation (e.g., as with TP10).

First, we consider the case of magainin 2. Figure 3.6a shows the time course of FI in the interaction of CF-magainin 2/magainin 2 with a single PG/PC (4/6)-GUV containing AF647 in its lumen (Karal et al. 2015). The FI of the GUV lumen due to AF647 started to decrease at 149 s, indicating that the membrane permeation of AF647 from the GUV started through a magainin 2-induced pore. On the other hand, the rim intensity due to CF-magainin 2 rapidly increased to a steady value,  $I_1$ , at  $t = 50$  s, remained constant for a long time ( $\sim 90$  s) until the intensity started to increase at a time similar to that of the start of membrane permeation of AF647, and then rapidly reached a final steady value,  $I_2$ . The average value of  $I_2/I_1$  is approximately 2.0. This result indicates that the steady binding of magainin 2 to the outer monolayer of the GUV membrane is attained at  $\sim 50$  s and the surface concentration of magainin 2 in the outer monolayer,  $X$ , remains constant until just before pore formation. Therefore, we can reasonably infer that the asymmetric transmembrane distribution of magainin 2 (i.e., localization of magainin 2 only in the outer monolayer) induces pore formation.

In contrast, the result for TP10 showed a different pattern. Figure 3.6b shows the time course of FI in the interaction of CF-TP10 with a single PG/PC-GUV containing AF647 in its lumen (Islam et al. 2014a). The rim intensity due to CF-TP10 gradually increased and reached a final, steady value at 125 s (Fig. 3.6b). On the other hand, the FI of the GUV lumen due to AF647 started to decrease at 212 s, indicating that the

membrane permeation of AF647 started through CF-TP10-induced pores. After pore formation, the rim intensity did not change. This result indicated that CF-TP10 translocates from the outer leaflet to the inner one from the beginning of the interaction, without pore formation; the steady binding of TP10 in both leaflets is achieved rapidly, and then after an extended time, pore formation occurs. Therefore, the symmetric transmembrane distribution of CF-TP10 (i.e., localization of CF-TP10 in both monolayers) induces pore formation. The AMPs with a type C MoA (e.g., LfcinB (4-9)) also can translocate across lipid bilayers without pore formation, but the symmetric distribution of these AMPs does not induce pore formation (Moniruzzaman et al. 2017).

The different relationship between the AMP-induced pore formation and the location of AMP in the membrane is due to the activity of translocation of AMPs across the lipid bilayer. This activity is more important for the CPPs, and various research have been performed on this topic (Madani et al. 2011; Islam et al. 2018). However, at present, the molecular mechanism of the translocation of peptides across the lipid bilayer is not clear, although several mechanisms have been proposed (Islam et al. 2018). The characteristics of peptides (e.g., hydrophobicity and amino acid sequence) required for translocation activity without pore formation also are not clear. Notably, the translocation activity depends not only on peptide properties but also on lipid bilayer properties. The presence of a high concentration of cholesterol in the bilayer greatly suppressed the translocation of CF-TP10 from the outer leaflet to the inner one, but higher concentrations of CF-TP10 induced pore formation in the same bilayer, through which CF-TP10 rapidly translocated across the bilayer (Islam et al. 2017). Therefore, the relationship between the CF-TP10-induced pore formation and the location of CF-TP10 in the bilayers containing high concentrations of cholesterol was almost the same as that of magainin 2 in PG/PC (4/6) membrane (Fig. 3.6a).

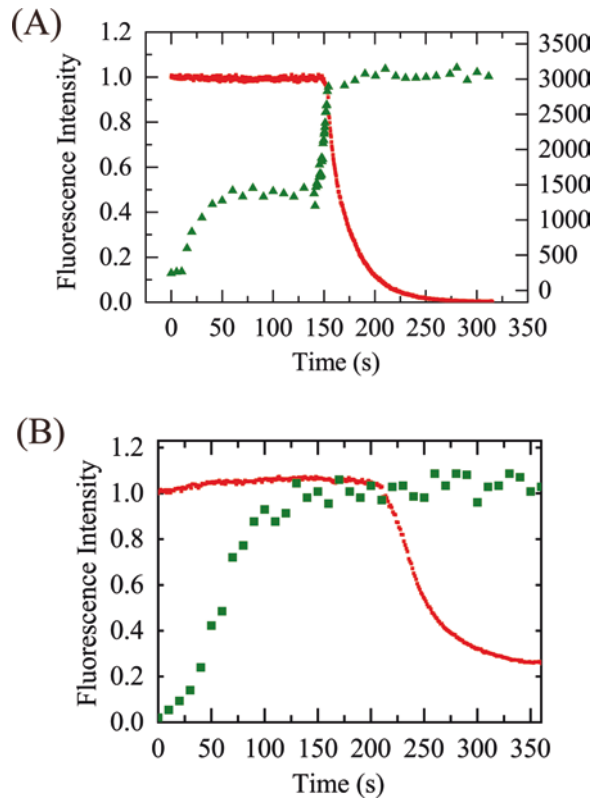


**Fig. 3.6** Relationship between the location of AMPs and pore formation. (a) Membrane permeation of AF647 and location of CF-magainin 2 in a PG/PC (4/6)-GUV. Time course of the change in FI due to AF647 and CF-magainin 2 of the GUV interacting with 31  $\mu\text{M}$  CF-magainin 2/magainin 2 is shown. The red squares and green triangles correspond to the normalized FI of AF647 inside the GUV (left axis) and the FI of CF-magainin 2 in the rim of the GUV (right axis), respectively. (b) Membrane permeation

of AF647 and location of CF-TP10 in a PG/PC (2/8)-GUV. Time course of the change in FI due to AF647 and CF-TP10 of the GUV interacting with 1.9  $\mu\text{M}$  CF-TP10 is shown. The red and green points correspond to the normalized FI of AF647 inside the GUV and of CF-TP10 in the rim of the GUV, respectively (a, b are reprinted from Karal et al. 2015; Islam et al. 2014a, respectively, with permission from the American Chemical Society)

### 3.5 Effect of Membrane Tension (or Stretching of Membranes) on AMP-Induced Pore Formation

#### 3.5.1 AMP-Induced Stretching of Lipid Bilayers and Membrane Tension

Generally, there is a possibility that the interaction with peptides/proteins such as AMPs affects the mechanical properties of plasma membranes and lipid bilayers. To measure the change in area of a GUV, we can use the micropipette aspiration method (Rawicz et al. 2000), where the GUV is fixed at the tip of the micropipette by a small

aspiration pressure, producing a small tension ( $\sigma \sim 0.5$  mN/m) in the GUV membrane. In the case of magainin 2, the fractional change in the area of a GUV membrane ( $\delta$ ) increased rapidly with time after the interaction of magainin 2 with the GUV started, reaching a steady value of  $\delta$  ( $\delta^{\text{ST}}$ ) within a short time ( $\sim 30$  s). The  $\delta^{\text{ST}}$  increased with an increase in magainin 2 concentration in the buffer,  $C$  (Fig. 3.7a) (Karal et al. 2015). After conversion of  $C$  to the surface concentration of magainin 2,  $X$  (mol/mol), the result indicated that  $\delta^{\text{ST}} \propto X$  (Fig. 3.7b). The combination of Figs. 3.1f and 3.7b indicated that the rate constant of magainin 2-induced pore formation ( $k_p$ ) had a positive correlation with  $\delta^{\text{ST}}$  (Fig. 3.7c). At a high concentration of magainin 2, during the steady

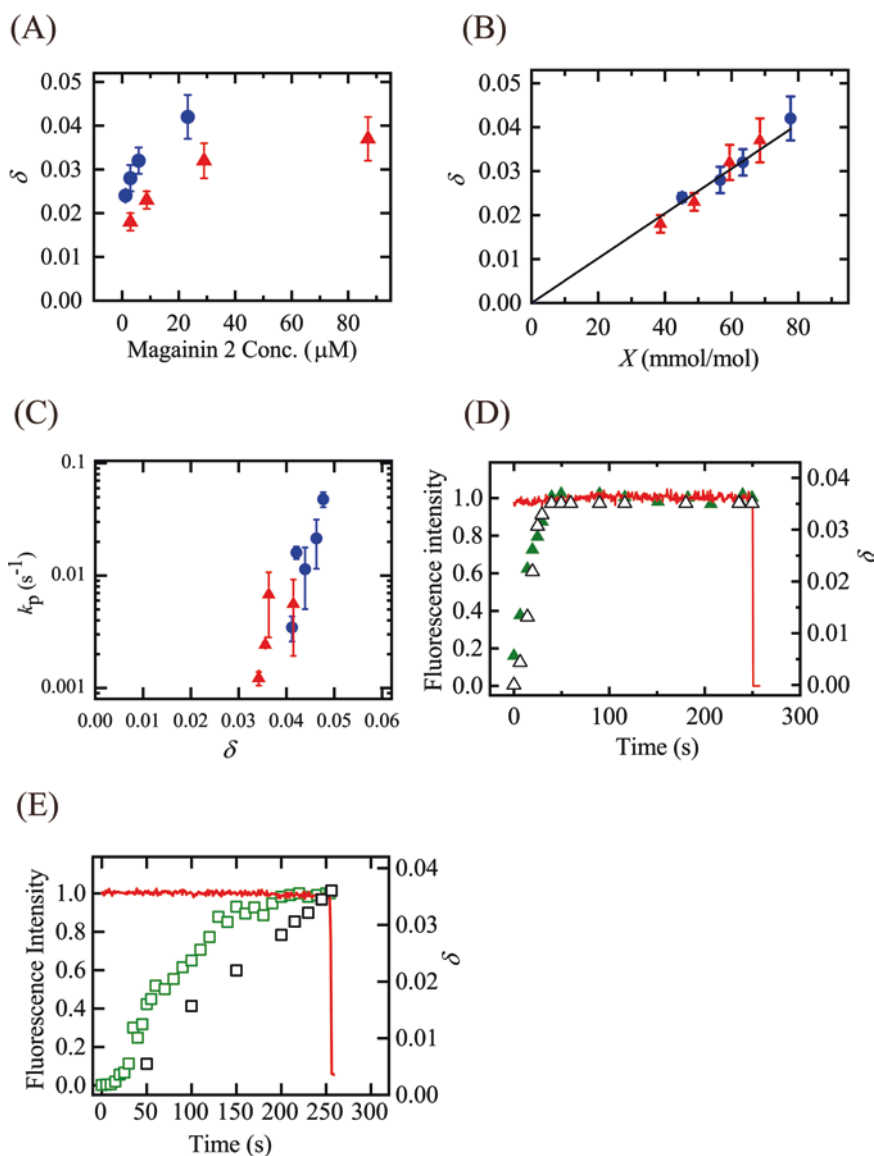


**Fig. 3.7** Effect of binding of AMP to a GUV on the membrane area. (a) The dependence of the fractional change in area of single GUVs,  $\delta$ , on the magainin 2 concentration in buffer A. (b) Dependence of  $\delta$  on the magainin 2 surface concentration,  $X$  (mmol/mol). (●) PG/PC (4/6)- and (▲) PG/PC (3/7)-GUV. (c) Dependence of  $k_p$  on  $\delta$  for magainin 2. (d) Time course of the FI of a PG/PC (4/6)-GUV and  $\delta$  interacting with 15  $\mu\text{M}$  CF-magainin 2 at  $\sigma = 0.5$  mN/m. Red line and green solid triangles represent the normalized FI of AF647 in the

GUV lumen and of CF-magainin 2 at its rim, respectively. Open triangles represent  $\delta$  (right axis). (e) Time course of the FI of a PG/PC (2/8)-GUV and  $\delta$  interacting with 0.3  $\mu\text{M}$  CF-TP10 at  $\sigma = 1.0$  mN/m. Red line and green squares correspond to FI of AF647 in the GUV lumen and of CF-TP10 at the rim of the GUV, respectively. Open squares represent  $\delta$  (a, b, d, and e are reprinted from Karal et al. 2015; Islam et al. 2017, respectively, with permission from the American Chemical Society)

state of stretching (i.e.,  $\delta = \delta^{\text{ST}}$ ), aspiration of GUV (which is induced by pore formation in the lipid bilayer) occurred stochastically. Figure 3.7d shows the result of the simultaneous measure-

ment of the magainin 2-induced change in the area, the rim intensity due to CF-magainin 2, and the membrane permeation of AF647 using CLSM. Both the rim intensity and  $\delta$  rapidly



increased to steady values within 50 s and then remained constant for a long time (~200 s) until pore formation. We could not detect any increase in the rim intensity just before pore formation (as shown in Fig. 3.6a), because the tension caused by the aspiration of a GUV by a micropipette increases the rate of opening (i.e., the increase in the radius) of the magainin 2-induced pore, and hence, the GUV is immediately aspirated into the micropipette after pore formation starts. This result indicated that the translocation of magainin 2 from the outer leaflet to the inner one occurred after pore formation, consistent with the inference that the asymmetric distribution of magainin 2 in the bilayer induces pore formation (Fig. 3.6a).

In contrast, in the case of TP10,  $\delta$  increased with time after the interaction of TP10 with the GUV started until aspiration of the GUV (Fig. 3.7e) (Islam et al. 2017). As the translocation of CF-TP10 from the outer leaflet to the inner one proceeds,  $\delta$  increases with time until pore formation. This result supports the idea that CF-TP10 translocates across the bilayer and that the binding of CF-TP10 in both monolayers induces their stretching.

### 3.5.2 Effect of Application of Tension Due to an External Force

We can control the membrane tension of single GUVs by applying an external force with micropipette aspiration (Evans et al. 2003; Levadny et al. 2013). This aspect is also one of the advantages of experimentation using single GUVs. Magainin 2-induced pore formation is affected greatly by membrane tension due to an external force; the rate constant of magainin 2-induced pore formation,  $k_p$ , increased with an increase in membrane tension (Karal et al. 2015). This result, as well as the result that the  $k_p$  increased with an increase in magainin 2-induced stretching of the bilayer, indicated that the magainin 2-induced pore is a stretch-activated pore (Karal et al. 2015). The membrane tension also increased the rate of translocation of CF-TP10 across the bilayer and that of CF-TP10-induced pore formation (Islam

et al. 2017). It is well known that the mechano-sensitive ion channels are activated when plasma membranes are stretched (Sukharev et al. 1994; Sachs 2010). Therefore, it will be useful to compare AMP-induced pore formation with the activation of the mechanosensitive channels.

### 3.5.3 Effect of Asymmetric Lipid Packing

The magainin 2-related results described in previous sections suggested that the stretching of the inner leaflet is a main driving force of magainin 2-induced pore formation (Karal et al. 2015). However, there was no direct experimental evidence for this hypothesis. Recently, Hasan et al. (2018a) developed a new method to prepare spherical GUVs with asymmetric lipid compositions in the two monolayers, such that a low concentration of lyso-PC (hereafter LPC) exists only in the inner leaflet (e.g., PG/PC/LPC (40/59/1; inner)-PG/PC (40/59; outer)-GUVs). In these GUVs, the lipid packing in the inner leaflet was larger than that in the outer one. Magainin 2-induced area increase ( $\delta^{ST}$ ) and the rate constant of magainin 2-induced pore formation ( $k_p$ ) decreased with increasing LPC concentration in the inner leaflet (i.e., the increase in asymmetric packing) (Hasan et al. 2018a). These results clearly support the idea that the stretching of the inner leaflet plays an important role in magainin 2-induced pore formation. Based on these results, we formulated a new quantitative theory on the initial stage of pore formation induced by magainin 2 (Hasan et al. 2018a). A theoretical equation of  $k_p$  as a function of magainin 2 surface concentration ( $X$ ) provided a good fit to the experimental results (Fig. 3.1f). This theory can explain the effect on  $k_p$  of the LPC concentration in the inner leaflet (Hasan et al. 2018a).

## 3.6 Concluding Remarks

In this mini-review, we summarized the present state of knowledge on the interactions of AMPs with lipid vesicles that were obtained using the

single GUV method. AMPs exhibit three MoAs on lipid bilayers. For a limited number of AMPs, we have obtained detailed information on the elementary processes of these MoAs, indicating that various processes are mediated by AMPs. On the basis of this information, we have proposed a mechanism for the initial stage of magainin 2-induced pore formation (Hasan et al. 2018a). However, we do not know the mechanism of the AMP-induced local rupture (type B MoA) and that of the entry of AMPs into the vesicle lumen (or bacterial cytoplasm) without pore formation (type C MoA). If we could examine other AMPs using single GUV methods, we might identify other kinds of MoAs and other elementary processes within the present MoAs. Further investigations of the MoAs of AMPs and the elementary processes of interaction of AMPs with lipid bilayers will be essential.

Even in the case of AMPs (such as magainin 2 and LfcinB) that attack the lipid membrane regions of bacterial and fungal plasma membranes, other factors of these microbial cells may affect the interaction of AMPs with the lipid membrane regions of the plasma membranes. However, we believe that these factors are additional to the fundamental characteristics of the interactions between AMPs and lipid bilayers. A close comparison between the results of interactions of AMPs with microbial cells and those of GUVs of lipid bilayers is expected to provide deeper insight into the elementary processes of action of AMPs and the mechanism of their antimicrobial activity.

## References

- Alam JM, Kobayashi T, Yamazaki M (2012) The single giant unilamellar vesicle method reveals lysenin induced pore formation in lipid membranes containing sphingomyelin. *Biochemistry* 51:5160–5172
- Baumgart T, Hess ST, Webb WW (2003) Imaging coexisting fluid domains in biomembrane models coupling curvature and line tension. *Nature* 425:821–824
- Bigay J, Antonny B (2012) Curvature, lipid packing, and electrostatics of membrane organelles: defining cellular territories in determining specificity. *Dev Cell* 23:886–895
- Bleicken S, Landeta O, Landajuela L, Basañez G, García-Sáez AJ (2013) Proapoptotic Bax and Bak proteins form stable protein-permeable pores of tunable size. *J Biol Chem* 288:33241–33252
- Evans E, Heinrich V, Ludwig F, Rawicz W (2003) Dynamic tension spectroscopy and strength of biomembranes. *Biophys J* 85:2342–2350
- Fuertes G, García-Sáez A, Esteban-Martin S, Giménez D, Sánchez-Muñoz OL, Schwille P, Salgado J (2010) Pores formed by Bax $\alpha$ 5 relax to a smaller size and keep at equilibrium. *Biophys J* 99:2917–2925
- Gregory SM, Pokorny A, Almeida PFF (2009) Magainin 2 revisited: a test of the quantitative model for the all-or-none permeabilization of phospholipid vesicles. *Biophys J* 96:116–131
- Hasan M, Karal MAS, Levadny V, Yamazaki M (2018a) Mechanism of initial stage of pore formation induced by antimicrobial peptide magainin 2. *Langmuir* 34:3349–3362
- Hasan M, Saha SK, Yamazaki M (2018b) Effect of membrane tension on transbilayer movement of lipids. *J Chem Phys* 148:245101
- Hwang PM, Vogel HJ (1998) Structure-function relationships of antimicrobial peptides. *Biochem Cell Biol* 76:235–246
- Islam MZ, Ariyama H, Alam JM, Yamazaki M (2014a) Entry of cell-penetrating peptide transportan 10 into a single vesicle by translocating across lipid membrane and its induced pores. *Biochemistry* 53:386–396
- Islam MZ, Alam JM, Tamba Y, Karal MAS, Yamazaki M (2014b) The single GUV method for revealing the functions of antimicrobial, pore-forming toxin, and cell-penetrating peptides or proteins. *Phys Chem Chem Phys* 16:15752–15767
- Islam MZ, Sharmin S, Levadny V, Shibly SUA, Yamazaki M (2017) Effects of mechanical properties of lipid bilayers on entry of cell-penetrating peptides into single vesicles. *Langmuir* 33:2433–2443
- Islam MZ, Sharmin S, Moniruzzaman M, Yamazaki M (2018) Elementary processes for the entry of cell-penetrating peptides into lipid bilayer vesicles and bacterial cells. *Appl Microbiol Biotechnol* 102:3879–3892
- Israelachvili JN (1992) *Intermolecular & surface forces*, 2nd edn. Academic, New York
- Karal MAS, Alam JM, Takahashi T, Levadny V, Yamazaki M (2015) Stretch-activated pore of antimicrobial peptide magainin 2. *Langmuir* 31:3391–3401
- Levadny V, Tsuboi T, Belaya M, Yamazaki M (2013) Rate constant of tension-induced pore formation in lipid membranes. *Langmuir* 29:3848–3852
- Lipowsky R, Sackmann E (eds) (1995) *Structure and dynamics of membranes*. Elsevier Science BV, Amsterdam
- Ludtke SJ, He K, Heller KH, Harroun TA, Yang L, Huang HW (1996) Membrane pores induced by magainin. *Biochemistry* 35:13723–13728
- Madani F, Lindberg S, Langel Ü, Futaki S, Gräslund A (2011) Mechanisms of cellular uptake of cell-penetrating peptides. *J Biophys* 2011:414729
- Matsuzaki K, Murase K, Fujii N, Miyajima K (1995) Translocation of a channel-forming antimicrobial pep-

- tide, magainin 2, across lipid bilayers by forming a pore. *Biochemistry* 34:6521–6526
- Matsuzaki K, Murase O, Fujii N, Miyajima K (1996) An antimicrobial peptide, magainin 2, induced rapid flip-flop of phospholipids coupled with pore formation and peptide translocation. *Biochemistry* 35:11361–11368
- Matsuzaki K, Sugishita K, Ishibe N, Ueha M, Nakata S, Miyajima K, Epanand RM (1998) Relationship of membrane curvature to the formation of pores by magainin 2. *Biochemistry* 37:11856–11863
- McLaughlin S, Murray D (2005) Plasma membrane phosphoinositide organization by protein electrostatics. *Nature* 438:605–611
- Melo MN, Ferre R, Castanho ARB (2009) Antimicrobial peptides: linking partition, activity and high membrane-bound concentrations. *Nat Rev Microbiol* 8:1–5
- Moghal MMR, Islam MZ, Sharmin S, Levadnyy V, Moniruzzaman M, Yamazaki M (2018) Continuous detection of entry of cell-penetrating peptide transport 10 into single vesicles. *Chem Phys Lipids* 212:120–129
- Moniruzzaman M, Alam JM, Dohra H, Yamazaki M (2015) Antimicrobial peptide lactoferricin B-induced rapid leakage of internal contents from single giant unilamellar vesicles. *Biochemistry* 54:5802–5814
- Moniruzzaman M, Islam MZ, Sharmin S, Dohra H, Yamazaki M (2017) Entry of a six-residue antimicrobial peptide derived from lactoferricin B into single vesicles and *Escherichia coli* cells without damaging their membranes. *Biochemistry* 56:4419–4431
- Müller P, Schiller S, Wiprecht T, Dathe M, Herrmann A (2000) Continuous measurement of rapid transbilayer movement of a pyrene-labeled phospholipid analogue. *Chem Phys Lipids* 106:89–99
- Nekhotiaeva N, Elmquist A, Rajarao GK, Hällbrink M, Langel C, Good L (2004) Cell entry and antimicrobial properties of eukaryotic cell-penetrating peptides. *FASEB J* 18:394–396
- Propheter DC, Chara AL, Harris TA, Ruhn KA, Hooper LV (2017) Resistin-like molecule  $\beta$  is a bactericidal protein that promotes spatial segregation of the microbiota and the colonic epithelium. *Proc Natl Acad Sci U S A* 114:11027–11033
- Qian S, Wang W, Yang L, Huang HW (2008) Structure of transmembrane pore induced by Bax-derived peptide: evidence for lipidic pores. *Proc Natl Acad Sci U S A* 105:17379–17383
- Rawicz W, Olbrich KC, McIntosh T, Needham D, Evans E (2000) Effect of chain length and unsaturation on elasticity of lipid bilayers. *Biophys J* 79:328–339
- Sachs F (2010) Stretch-activated ion channels: what are they? *Physiology* 25:50–56
- Sandre O, Moreaux L, Brochard-Wyart F (1999) Dynamics of transient pores in stretched vesicles. *Proc Natl Acad Sci U S A* 96:10591–10596
- Sukharev SI, Blount P, Martinac B, Blattner FR, Kung C (1994) A large-conductance mechanosensitive channel in *E. coli* encoded by *mscL* alone. *Nature* 368:265–268
- Tamba Y, Yamazaki M (2005) Single giant unilamellar vesicle method reveals effect of antimicrobial peptide, magainin 2, on membrane permeability. *Biochemistry* 44:15823–15833
- Tamba Y, Yamazaki M (2009) Magainin 2-induced pore formation in membrane depends on its concentration in membrane interface. *J Phys Chem B* 113:4846–4852
- Tamba Y, Ohba S, Kubota M, Yoshioka H, Yoshioka H, Yamazaki M (2007) Single GUV method reveals interaction of tea catechin (-)-epigallocatechin gallate with lipid membranes. *Biophys J* 92:3178–3194
- Tamba Y, Ariyama H, Levadny V, Yamazaki M (2010) Kinetic pathway of antimicrobial peptide magainin 2-induced pore formation in lipid membranes. *J Phys Chem B* 114:12018–12026
- Tanaka T, Sano R, Yamashita Y, Yamazaki M (2004) Shape changes and vesicle fission of giant unilamellar vesicles of liquid-ordered phase membrane induced by lysophosphatidylcholine. *Langmuir* 20:9526–9534
- Wade D, Boman A, Wahlin B, Drain CM, Andreu A, Boman HG, Merrifield RB (1990) All-D amino acid-containing channel-forming antibiotic peptides. *Proc Natl Acad Sci U S A* 87:4761–4765
- Wakabayashi H, Matsumoto H, Hashimoto K, Teraguchi S, Takase M, Hayasawa H (1999) N-acylated and D enantiomer derivatives of a nonamer core peptide of lactoferricin B showing improved antimicrobial activity. *Antimicrob Agents Chemother* 43:1267–1269
- Yamazaki M (2008) The single GUV method to reveal elementary processes of leakage of internal contents from liposomes induced by antimicrobial substances. *Adv Planar Lipid Bilayers Liposomes* 7:121–142
- Yang LT, Weiss M, Lehrer RI, Huang HW (2000) Crystallization of antimicrobial pores in membranes: magainin and protegrin. *Biophys J* 79:2002–2009
- Zaslouf M (2002) Antimicrobial peptides of multicellular organisms. *Nature* 415:389–395